Journal of Cranio-Maxillo-Facial Surgery 53 (2025) 1647–1655

Contents lists available at ScienceDirect

Journal of Cranio-Maxillo-Facial Surgery

journal homepage: www.jcmfs.com

Impact-resistance of bio-inspired functionalized polyether-ether-ketone implant for cranioplasty

Dylan Coyle [a,b], Bianca Zumbo [a,b,d,*], Niko Moritz [a,b], Janek Frantzén [c], Kalle Aitasalo [e], Gianluca Turco [d], Julia Kulkova [a,b]

[a] Biomedical Engineering Research Group, Biomaterials and Medical Device Research Program, Itäinen Pitkäkatu, 4B PharmaCity, 20520, Turku, Finland
[b] Department of Biomaterials Science and Turku Clinical Biomaterials Centre – TCBC, Institute of Dentistry, University of Turku, Itäinen Pitkäkatu 4B, PharmaCity, 20520, Turku, Finland
[c] Clinical Neurosciences, Department of Neurosurgery, Turku University Hospital, University of Turku, Turku, Finland
[d] Clinical Department of Medical, Surgical and Health Sciences, University of Trieste, 34100, Trieste, Italy
[e] Professor Emeritus, Department of Otorhinolaryngology-Head and Neck Surgery, Division of Surgery and Cancer Diseases, Turku University Hospital, University of Turku, Turku, Finland

ARTICLE INFO

Keywords:
3D-printing
Additive manufacturing (AM)
Cranial implants
Finite element analysis (FEA)
Mechanical testing
PEEK (polyether ether ketone)

ABSTRACT

This study introduces Amanita, a pioneering bionic design for a fully 3D-printed cranial implant made of polyether-ether-ketone (PEEK) functionalized with bioactive glass granules. The mechanical integrity of cranial implants is crucial for effective brain protection. The primary aim was to evaluate the mechanical resistance of this innovative implant to validate its functionality for cranial protection. We employed a standardized biomechanical testing protocol to assess the mechanical properties of the Amanita implants. The implants were subjected to impact forces that simulated real-life blunt trauma scenarios to test their performance under stress. The Amanita implants exhibited significant resilience under compressive forces, withstanding over 100 N at a 2 mm deflection and effectively absorbing more than 1000 mJ at a 6 mm deflection. Furthermore, these implants maintained structural integrity without catastrophic failure at deflections up to 10 mm. The findings validate the design and manufacturing approach of the Amanita implants, demonstrating their potential for clinical use in cranioplasty. The implants showed adequate impact resistance, potentially lowering the risk of injury from falling objects or blunt trauma. Additionally, the adoption of additive manufacturing techniques enables the production of these implants on-site at hospitals, promoting socially and environmentally sustainable healthcare solutions.

1. Introduction

Cranioplasty, an established surgical procedure aimed at the reconstruction of cranial defects typically resulting from trauma, tumor resections, infections, or congenital anomalies (Aydin et al., 2011; Mah and Kass, 2016). This procedure restores brain protection and addresses aesthetic outcomes. The durability of implants is critical to prevent breakage from impacts (Jaberi et al., 2013; Di Cosmo et al., 2025). Moreover, a major concern is the risk of infection (De Bonis et al., 2012; Khalid et al., 2022; Magni et al., 2024), highlighting the importance of selecting appropriate materials and designs to reduce this risk (Kauke-Navarro et al., 2024).

While additive manufacturing (AM) is well-established for creating patient-specific implants (PSIs), particularly in cranial reconstructions, where simple geometries are prevalent, its capabilities extend significantly beyond these applications (Pöppe, Johannes P. et al., 2024). AM allows for the fabrication of structurally complex implants and the integration of diverse materials. This technique has been effectively employed in fields such as orthopedics and dental implantology, where multifaceted designs and material composites are used to enhance functionality and biocompatibility (Cong and Zhang, 2025). Such advanced applications of AM have not yet been fully utilized in the development of cranioplasty implants, presenting a promising area for innovative research and application. The adoption of bionic designs in

* Corresponding author. Department of Medical, Surgical and Health Science, University of Trieste, 34100, Trieste, Italy.
E-mail addresses: dylan.coyle@utu.fi (D. Coyle), bianca.zumbo@phd.units.it (B. Zumbo), niko.moritz@utu.fi (N. Moritz), janfra@utu.fi (J. Frantzén), kalaita@utu.fi (K. Aitasalo), gturco@units.it (G. Turco), Julia.kulkova@utu.fi (J. Kulkova).

https://doi.org/10.1016/j.jcms.2025.06.009
Received 3 February 2025; Received in revised form 21 May 2025; Accepted 15 June 2025
Available online 17 July 2025

cranioplasty implants, however, remains underexplored and represents a promising area for innovative research and application (Sharma et al., 2021b).

In this work, we present a concept for a cranial implant that integrates bionic principles and AM, using a combination of PEEK (Punchak et al., 2017; Van De Vijfeijken et al., 2018; Zhang et al., 2018; Sun et al., 2022) and bioactive glass S53P4 (BAG). The design aims to provide mechanical strength and biological integrity with soft tissues (Miguez-Pacheco et al., 2015; Zhao et al., 2008) and bone (Lindfors et al., 2010b; Välimäki and Aro, 2006), with the potential for antibacterial properties attributed to the BAG (Lindfors et al., 2010a; Munukka et al., 2008). However, this paper focuses primarily on the mechanical properties of the design. Additionally, our manufacturing process is designed to be material-efficient, printing the implant flat and shaping it post-production, which may reduce both time and costs.

2. Materials and methods

2.1. Predicate devices

The primary predicate device was Glace (Skulle Implants Oy, Finland), a glass-fibre reinforced composite pouch consisting of laminated layers of woven glass fibre fabrics embedded in a bisphenol A glycidyl methacrylate (BisGMA)–triethylene glycol dimethacrylate (TEGDMA) matrix (Aitasalo et al., 2014). The implant features an impervious outer surface interfacing with the skin and a porous inner surface interfacing with the dura. The pouch is filled with BAG granules to enhance osteointegration (Piitulainen et al., 2017; Vallittu et al., 2020). Another predicate device was OSSDESGN cranial implant (OssDsign AB, OSSDSIGN Cranial PSI, (510(k))., 2021), which incorporates a unique design with a 3D-printed titanium skeleton embedded within calcium phosphate (CaP) ceramic tiles Persson et al. (2018); (OssDsign AB, OSSDSIGN Cranial PSI, (510(k))., 2021). Both devices, functionalized with BAG and CaP respectively, are onlay types and have a substantial history of clinical use, making them relevant benchmarks in this study. Moreover, both devices are expected to exhibit antibacterial properties due to the well-documented efficacy of BAG and the potential for doping CaP with antibiotics, as described by Sundholm et al. (Sundblom et al., 2019)

2.2. Design and methodology

Implant Design Overview: The Amanita cranial implant is an "onlay" type that covers both the bone defect and a strip of adjacent cranial bone. It combines AM techniques and material science, featuring a bionic design inspired by the Amanita mushroom. This design mimics the mushroom's curved cap and spotted pattern, which enhances its functionality and aesthetic appeal. The implant facilitates ease of use for surgeons and integrates aesthetically with patient anatomy.

Mechanical Design: The implant includes a lattice structure with BAG granules, providing structural integrity and impact dissipation (Fig. 1A). The hexagonal Truchet pattern, arranged at a 60-degree angle, reduces rigidity and allows for shaping flexibility (Fig. 1B). It also includes 12 screw holes for secure fixation and is adaptable to both standard and patient-specific variations (Fig. 1C).

Manufacturing Process: Produced through 3D printing in a flat

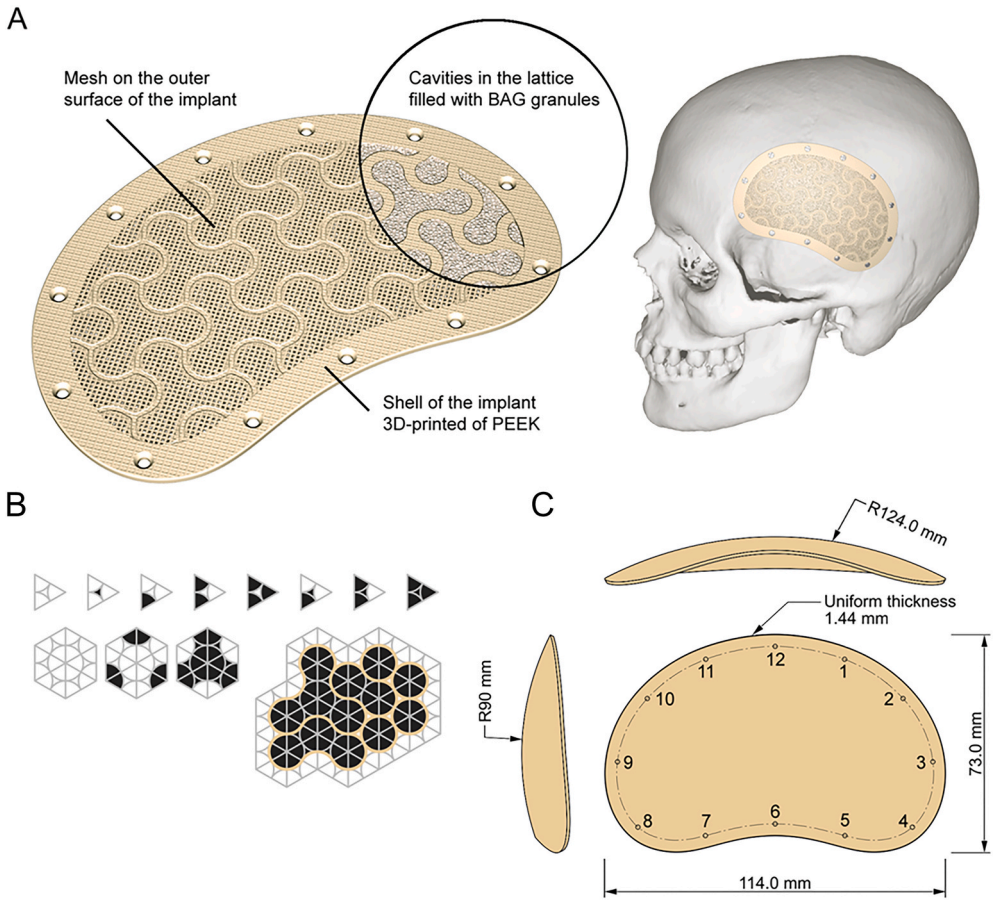

Fig. 1. Design and dimensions of the Amanita implant: A) Design of the implant based on the underlying lattice; B) The lattice design features a pattern of circles arranged at a 60-degree angle. When modeled as a hexagonal Truchet pattern these circles can be merged to form clusters of up to four circles (adapted from Kulkova, 2023); C) Dimensions and arrangements for screw fixation, tested with screws fixed in three configurations: '12' - all holes used, and alternately in two patterns, '6 odd' (1, 3, 5, 7, 9, 11) and '6 even' (2, 4, 6, 8, 10, 12), with the other holes left empty.

configuration, the implant undergoes post-production shaping through a specialized forming process. This approach supports rapid customization to fit various cranial shapes and reduces manufacturing time and material use.

Biological Performance: The lattice design enhances mechanical strength while promoting biological integration. BAG granules are incorporated within the cavities of the lattice and are secured by the mesh at the outer surface of the implant (Fig. 1). Unlike the Glace implants, Amanita implants are designed to isolate BAG granules from the dura, interfacing instead with the skin flap through a meshed outer surface. This arrangement is intended to promote the integration of soft tissues into the implant (Zhao et al., 2008), potentially facilitating attachment to the vascularized tissue flap. Additionally, considering that the primary route of infection, such as in surgical site infections, typically originates from the outer surface that interfaces with the skin and not the side facing the dura and brain, strategically exposing BAG granules on the skin-facing side may offer greater benefits. The osteointegration potential of PEEK doped with biphasic calcium phosphate (Evonic CaP-Loaded Vestakeep) could enhance the osteoconductive properties of Amanita implants. The design's potential for better soft tissue integration remains to be empirically verified.

Design Aesthetics and Functionality: Reflecting natural forms, the bionic design of the Amanita implant is tailored to merge functionality with aesthetics. The flexibility to adapt from flat to curved forms mirrors the natural variability found in mushroom caps. This approach focuses on patient aesthetics and simplifies surgical procedures, blending natural inspiration with medical functionality.

Development Stages: In the first stage, the mechanical properties of 3D-printed PEEK specimens were evaluated through three-point bending tests to establish parameters for simulation models in Finite Element Analysis (FEA). These tests were then simulated using FEA to develop a working model for subsequent simulations of actual implant shapes. In the second phase, FEA was utilized to screen potential Amanita implant designs by simulating their performance under impact conditions. In the third phase, once a single implant design was selected, it was 3D-printed and underwent physical mechanical testing.

2.3. Assessment of mechanical properties for FEA

Mechanical properties of 3D-printed PEEK specimens were evaluated in three-point bending tests, following the standards outlined in ISO 178:2019. Specimens, measuring 65 mm in length, 10 mm in width, and 3.3 mm in thickness, were 3D-printed using Apium P220 3D printer (Apium Additive Technologies GmbH, Germany), equipped with a 0.2 mm nozzle, utilizing PEEK filament (Evonik), and layer thickness at 0.1 mm. During printing, the filament was maintained at 120 °C in a filament dryer.

Two types of specimens (N = 5 for each type) were tested: one with a completely solid structure and another featuring a 65 % grid infill pattern, intended to mimic the implant's mesh structure. The grid infill consisted of intersecting lines at 90° to each other. A universal mechanical testing machine (Lloyd Instruments, UK) was used for testing. The specimens were positioned with a span of 50 mm between supports with the loading applied at a speed of 1 mm/min. Load-deflection curves were subsequently used to inform FEA parameters.

2.4. Screening of Amanita implant designs by FEA

Three-point bending tests were recreated in SolidWorks (Dassault Systèmes). In this simulation, mechanical properties and settings derived from physical tests were applied, including a bending modulus of 2900 MPa for solid PEEK and 800 MPa for grid-infilled PEEK, complemented by a Poisson's ratio of 0.4, aligning with values reported in recent studies (Liaw et al., 2021; Wang et al., 2021). These parameters were assumed to be linear elastic and isotropic as validated by previous research (Huys et al., 2021).

Four implant designs were selected for screening as illustrated in Fig. 2: Solid PEEK, a uniformly solid structure; Amanita O, featuring a lattice of cavities; Amanita I, incorporating a transverse reinforcing element; and Amanita X, which included two cross-linked diagonal reinforcing elements. All reinforcing elements were comprised of solid PEEK. The implant designs were based on the kidney-shaped design introduced by Piitulainen et al. (2017) to allow direct comparison to their data. The Amanita designs were created using Rhinoceros 7 CAD software (Robert McNeel & Associates, USA) with parametrization by Grasshopper for their implementation as PSIs.

FEA was performed to simulate the mechanical test described by Piitulainen et al. (2017) by applying a static load perpendicular to a 30 mm-diameter circular area at the implant's geometric centre, simplifying real-life scenarios. Essentially, this test is similar to the FEA setup used by Persson et al. (2018). Screw fixation configurations were also evaluated, with implants featuring 12 screw holes arranged like a clock face. Configurations tested included all 12 screws, and two alternating patterns using 6 screws each: '6 odd' (1, 3, 5, 7, 9, 11) and '6 even' (2, 4, 6, 8, 10, 12). The goal was to identify a design that performed well, regardless of the screw fixation pattern. The yield stress for PEEK was set at 94 MPa (Evonic Vestakeep I4).

2.5. Mechanical testing of Amanita implants

The implants were 3D-printed using the equipment materials described above for printing the specimens. The printing process, performed layer by layer, started from the meshed outer surface of the implant that interfaces with the skin, progressing towards the inner surface interfacing with the dura. After printing the lattice structure, the process was paused and BAG granules (S53P4, fraction 300–500 μm, BonAlive Biomaterials Oy, Finland) were inserted into the cavities using a purpose-made tool. Printing was resumed to create a solid PEEK barrier between the BAG granules and the inner surface of the implant. Subsequently, the implants underwent post-treatment at 150 °C to achieve spatial shaping into the desired 3D curvatures.

Mechanical testing followed the protocol and equipment outlined by Piitulainen et al. (2017), facilitating direct comparison with the study's findings. Amanita implant was directly compared with glass-fibre reinforced Glace implants. Amanita X implants (N = 5) were secured with six screws to a custom aluminum jig replicating a typical cranial defect and subjected to compression at a constant speed of 1 mm/min using a universal testing machine (LR30K, Lloyd Instruments Ltd, UK). Force measurements were recorded up to a 10-mm deflection across five samples. Compressive force and energy absorption were calculated from the force-deflection curves using Origin 2016 (OriginLab Corp., USA). Statistical analysis was conducted with IBM SPSS Statistics v26, starting with a Kolmogorov-Smirnov test for normal distribution, followed by an ANOVA and Tukey post-hoc test to compare results with those of by Piitulainen et al. (2017), considering a significance level of $P < 0.05$.

3. Results

3.1. Screening of Amanita implant designs by FEA

Based on FEA analysis, Amanita X was selected for implementation in physical form for actual mechanical testing due its lower sensitivity to variations in screw fixation patterns and its ability to withstand loads up to 300 N without exceeding the yield stress of PEEK. Fig. 3 shows the von Mises stress distribution for different Amanita designs under a 300 N load, highlighting non-uniform stress distribution with areas of high stress concentration that could precipitate failure. Fig. 4 presents graphs of maximum von Mises stress and strain against loads ranging from 100 N to 400 N. Under a 300 N load, Amanita O and Amanita I exhibited potential failure points in '6 even' and '12′ screw configurations, while Amanita X maintained structural integrity. Notably, '6 even' configurations showed higher stresses and strains compared to '6 odd' and '12′,

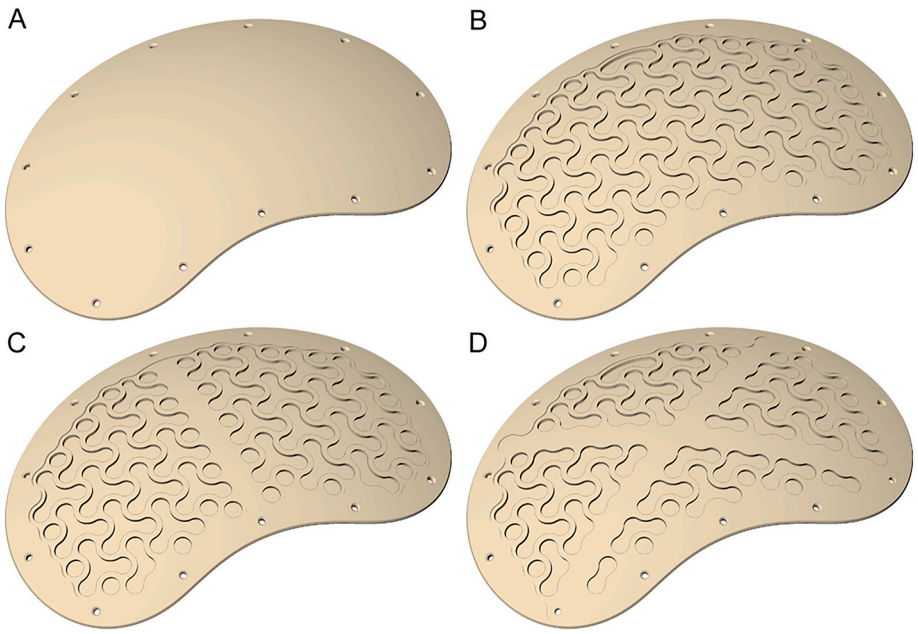

Fig. 2. Four implant designs selected for screening: A) Solid PEEK; B) Amanita O with a lattice of cavities; C) Amanita I with a lattice of cavities with a transverse reinforcing element; D) Amanita X with a lattice of cavities with two cross-linked diagonal reinforcing elements.

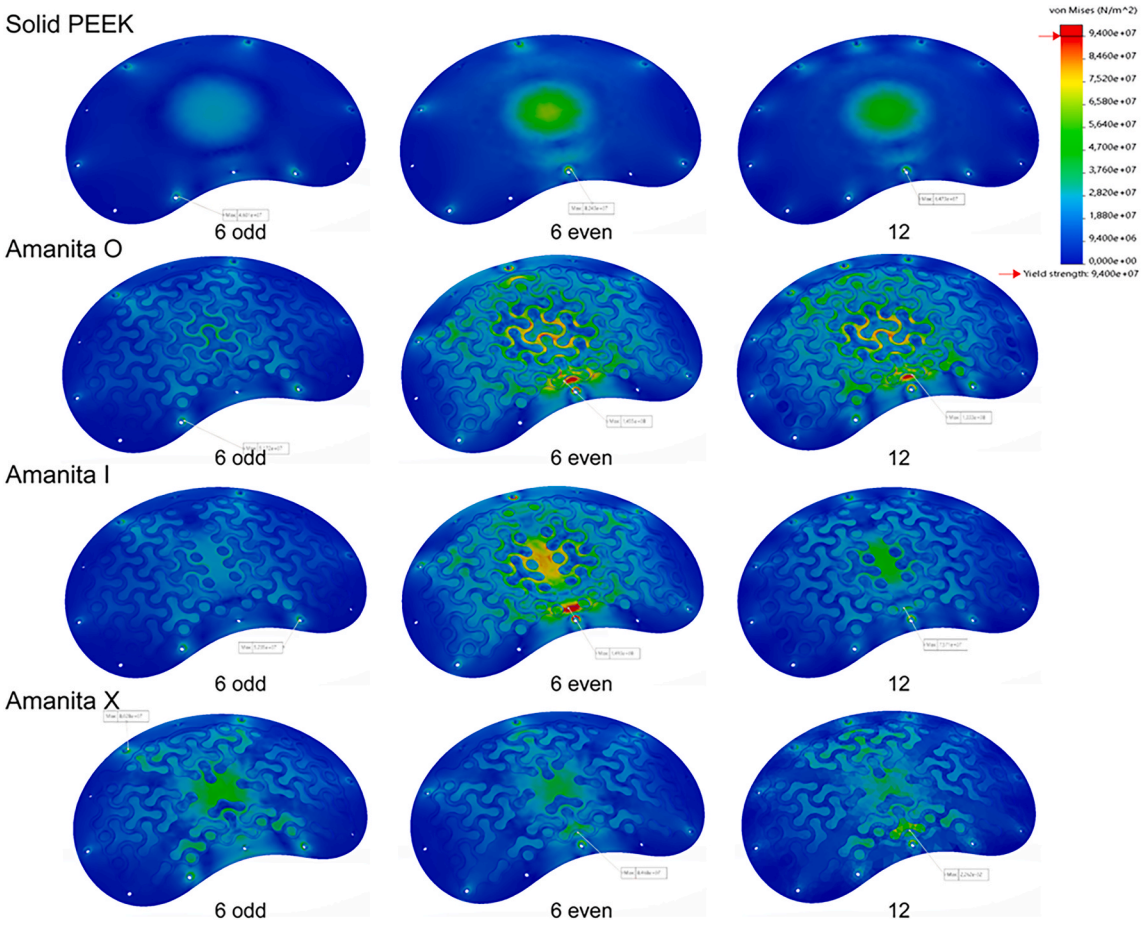

Fig. 3. von Mises stress patterns for various Amanita implant designs under a load of 300 N tested with screws fixed in three configurations. The mesh on the outer surface of the implant is not shown for clarity.

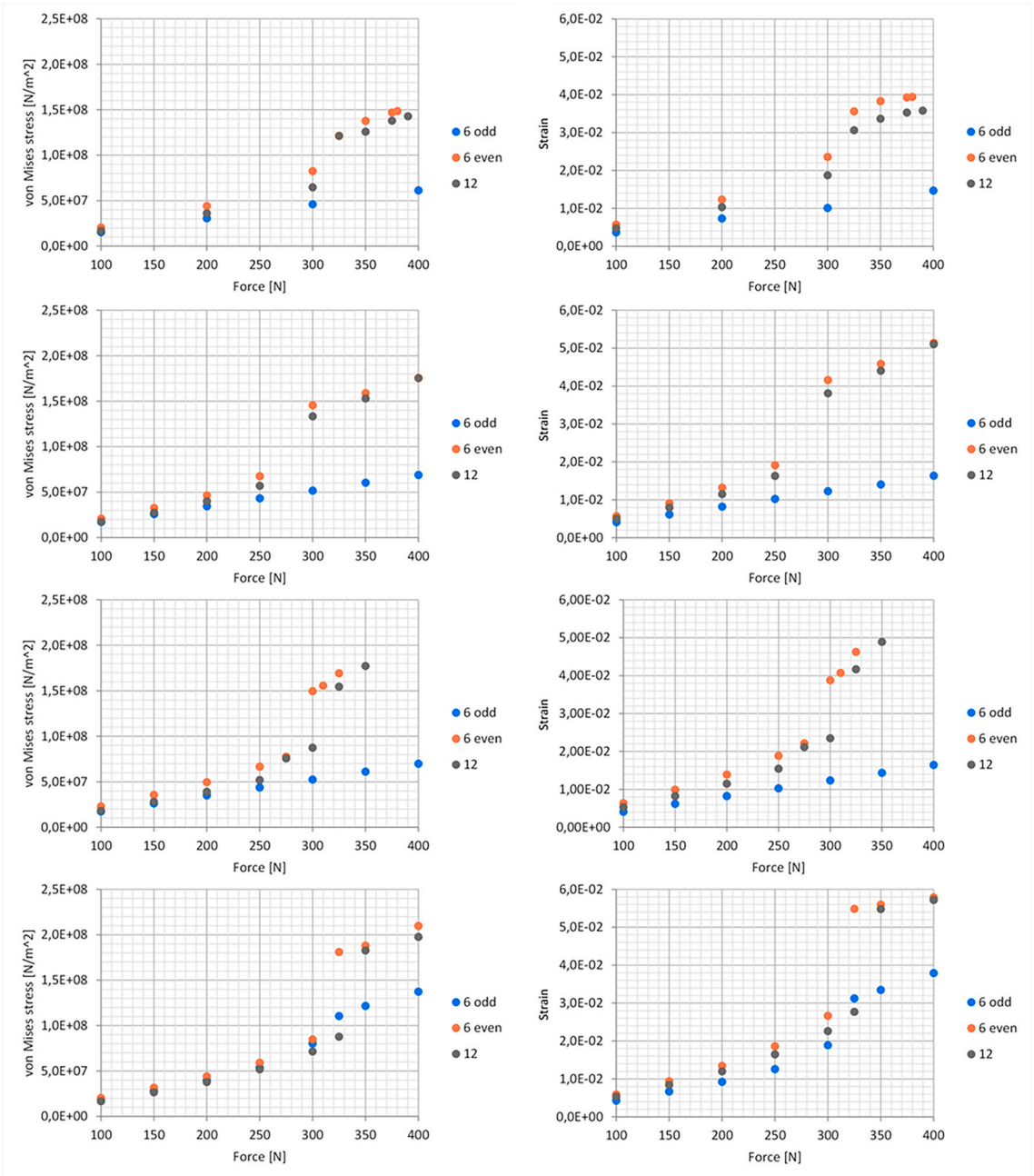

Fig. 4. Maximal von Mises stress and strain as functions of the applied load.

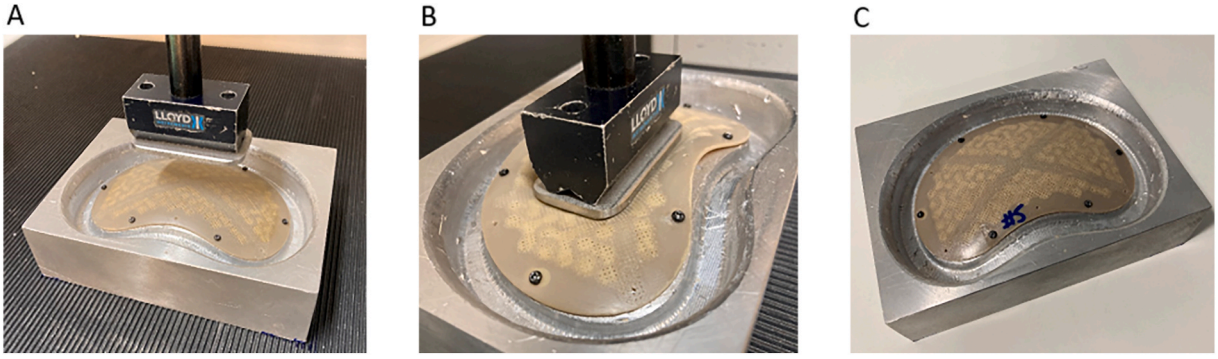

Fig. 5. Compressive testing of Amanita implants. A) Prior to the test, B) Plunger penetrating the surface to a displacement of 10 mm and C) View of the implant after the removal of the plunger.

influenced by screw positioning and implant geometry.

3.2. Mechanical testing of Amanita implants

The mechanical performance of the novel Amanita implants was analyzed and compared with Piitulainen et al.'s study, which evaluated the equivalents of glass-fibre reinforced Glace implants, specifically focusing on their Group 4 due to its identical experimental setup to ours and thus serving as a control group in our study. However, we extended the analysis beyond the original scope to include energy absorption alongside compressive force, measuring both at incremental 1 mm deflections up to 6 mm.

During testing, the Amanita implants exhibited partial delamination at a 10 mm deflection; however, this did neither result in catastrophic failure of the implant nor the escape of the bioactive glass granules from the cavities Fig. 5 provides a visual illustration of Amanita implants under compression testing. The compressive force results are represented in Fig. 6 using a boxplot, a standardized method of displaying data distribution.

Following the confirmation of a normal distribution through the Kolmogorov-Smirnov test, the data was evaluated using a parametric ANOVA test. Statistically significant differences between the data from Piitulainen et al. and the data for the Amanita implants were observed at 2 mm ($P = 0.048$), 3 mm ($P < 0.001$), 4 mm ($P < 0.001$), 5 mm ($P < 0.001$), and 6 mm ($P < 0.001$) deflection steps.

The same approach was applied to assess absorbed energy, with results represented in Fig. 7 in a boxplot format. Following the affirmation of a normal data distribution by the Kolmogorov-Smirnov test, a parametric ANOVA test was performed. This test revealed statistically significant differences between the Glace implants and the Amanita implants at 3 mm ($P < 0.026$), 4 mm ($P < 0.001$), 5 mm ($P < 0.001$), and 6 mm ($P < 0.001$) deflection steps.

4. Discussion

The primary objective of this study was to introduce a design of a novel cranial implant that incorporates bionic principles and AM utilizing a combination of PEEK and S53P4 bioactive glass. This integration aimed to combine durability, antibacterial properties, and on-site manufacturing capabilities within a single device. From a mechanical standpoint, Amanita implants demonstrated the ability to withstand considerable compressive forces and absorb significant energy before failure. These properties meet the essential requirements for patient safety and effectiveness in cranial reconstructive surgery, as assessed from regulatory, biomechanical, and comparative implant perspectives.

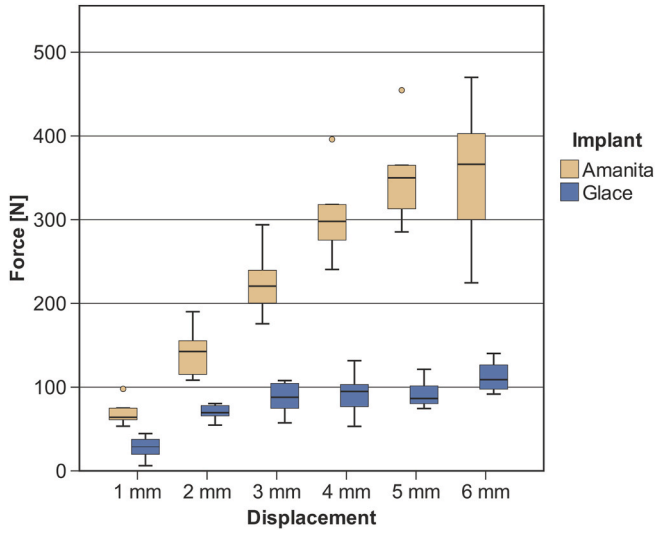

Fig. 6. Comparison of Amanita implants and control implants in terms of compressive force measured at 1 mm deflection step.

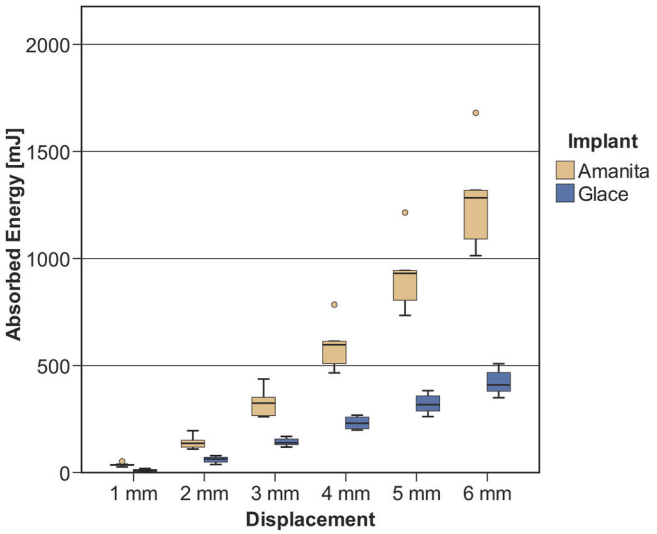

Fig. 7. Comparison of Amanita implants and control implants in terms of absorbed energy measured at 1 mm deflection step.

Mechanical testing is a crucial part of the implant certification process, as per the regulations of health authorities. Frequently, a pre-existing or 'predicate' device is used as a benchmark to certify a new device, a process commonly seen in regulatory pathways like the 510(k) clearance with U.S. Food and Drug Administration (FDA). For example, OSSDSIGN Cranial PSI successfully passed FDA certification, assessing its ability to withstand dynamic loads, resist high forces, absorb substantial energy, and maintain shape under force (OssDsign AB, OSSDSIGN Cranial PSI, (510(k))., 2021).

The Maximum Force Test required the PSI to endure forces greater than 100 N, simulating protection against impacts like falling objects and blunt trauma. The Energy Absorption Test demonstrated the PSI's ability to absorb more than 1000 mJ of energy before failure, offering another measure of protective capacity. The Resistance to Deformation Test assessed the PSI's structural integrity, allowing no more than 6 mm deformation under a force of 100 N. These benchmarks were integral to our study.

The compressive testing results show that Amanita implants can withstand compressive forces exceeding 100 N at a 2 mm deflection, and over 200 N at a 3 mm deflection. Despite early signs of delamination at a 3 mm deflection, these implants did not fail catastrophically, even at a deflection of 10 mm. At 6 mm, Amanita implants are capable of absorbing more than 1000 mJ of energy, in accordance with the Maximum Force Test requirements described previously.

It is important to note that Piitulainen et al. did not originally perform calculations for energy absorption; this analysis was added by us, utilizing the available raw data as co-authors of the study. Both Amanita and the control Glace implants are "on-lay" types filled with BAG granules and underwent similar testing procedures. Given the extensive clinical use and successful implantation of over 2000 Glace implants, comparing them with Amanita is clinically relevant. The testing affirmed that Amanita implants withstand significantly higher compressive forces and absorb more energy than the control implants, starting from a deflection of 2 mm.

To understand the clinical relevance of our findings, we must consider previously reported force-deformation characteristics and energy absorption measurements associated with human skulls and cranial implants from the literature. As per Van Lierde et al. (2003), the average values were 1975 ± 703 N for peak force, 4.17 ± 0.81 mm for maximum deformation, and 3.95 ± 1.18 J for absorbed energy to fracture, reflecting the natural variability in individual skulls. Amanita implants'

performance metrics are within these ranges.

Ono et al. (1998) suggested that cranial implants should resist at least 200 N of force to prevent failure, a threshold our Amanita "on-lay" implants meet at a 3 mm deflection. However, this comparison must consider design differences, as Amanita "on-lay" implants, which cover the defect and adjacent bone, are structurally distinct from the "in-lay" hydroxyapatite implants of their study which fill the bone defect and receive less structural support. Additionally, "on-lay" implants are usually thinner (1–3 mm) than "in-lay" ones (3–6 mm), making direct mechanical testing comparisons potentially speculative.

Sharma et al. (Sharma et al., 2021a) tested mechanical properties of in-lay PEEK cranial implants, typically measuring 3–5 mm in thickness, produced with a 3D printer similar to ours. Their method involved a spherical plunger with a 10 mm diameter and resulted in catastrophic failure at 798.38 ± 211.45 N force and 2.54 ± 0.56 mm displacement. However, these results are not directly comparable to our Amanita implant data due to differences in implant types and test setups.

Berretta et al. (2018) conducted mechanical testing on "in-lay" PEEK cranial implants, fabricated using a high-temperature laser sintering additive manufacturing process in varied orientations. They used a testing setup similar to ours, albeit with a spherical plunger of unspecified diameter. The implant failure was observed at around 7 mm displacement, with force ranges from approximately 150 to 720 N depending on the manufacturing orientation. The force values at various displacements were observed to be around 25 N at 2 mm, 50 N at 3 mm, 100 N at 4 mm, 150 N at 5 mm, and 280 N at 6 mm. The reported energy absorption prior to failure was roughly between 1200 and 2400 kJ, an amount that appears exceedingly high compared to typical requirements and may likely be a reporting error in the order of magnitude, possibly intended to be mJ instead of kJ. However, a direct comparison of these results with those of our Amanita implants isn't feasible due to the differences in implant types and testing methodologies.

The statistical significance of the results suggested that the Amanita implants differed from the predicate implants tested in their ability to withstand compressive forces and absorb energy under experimental conditions.

We did yet not attempt complex FEA simulations as reported (Huys et al., 2021; Marcián et al., 2019; Moiduddin et al., 2023) our goal was screening, applying FEA in preliminary design stages for screening potential implant designs. It allows for rapid visualization of stress and strain distributions without the need for physical prototypes at every iteration. This aspect is crucial for eliminating designs that clearly do not meet mechanical requirements or optimizing configurations before expensive and time-consuming physical tests are conducted. One of the main challenges with FEA in this context is accurately simulating the complex interactions within a dynamic biological environment. An implant isn't just a static object; it's part of a system that includes the varied anatomy of human bone, the variability in surgical placement, and the mechanical interactions with fixation devices like screws. Moreover, the physical act of loading an implant during testing (e.g., with a plunger) introduces additional variables that are difficult to model accurately. These include interaction between the implant, screws, and jig during physical tests can lead to localized stresses that are hard to precisely replicate in FEA due to the complexities of accurately modelling contact forces and friction. There is a risk that the pursuit of perfectly aligned virtual and physical test results becomes an academic exercise, detracting from the goal of improving clinical outcomes. While academic exploration of these technologies is valuable, it is crucial to maintain a focus on their practical, clinical implications.

In critical applications, working strains must remain well below the yield point to ensure reliability and prevent plastic deformation. For PEEK, where yield stress of 94 MPa is close to its tensile strength of 94 MPa, and stress at break of 76 MPa (Evonic Vestakeep I4), material failure may occur immediately upon exceeding these limits, as indicated by FEA analysis (Fig. 4). In Amanita cranial implants, however, high stresses and strains were localized at screw fixation points. This does not suggest catastrophic failure of the implant but rather localized failure at the screws, which is less critical and does not compromise the implant's ability to protect the brain. This observation was corroborated by actual mechanical tests.

The X-shaped reinforcement (Fig. 3) improves load distribution and impact resistance, though its effectiveness depends on impact direction and location. FEA results also highlight the critical influence of screw fixation patterns on implant stability, offering valuable insights for clinicians regarding mechanical performance in cranial implants.

Trends in cranial reconstruction include on-site 3D printing of PSIs in hospitals (e.g., Skåne University Hospital, Sweden, and University Hospital Basel, Switzerland) (Ebel et al., 2023), bio-inspired generative design (Sharma et al., 2021b), designer biomaterials (Zadpoor, 2020; Elshazly et al., 2024), and automated implant reconstruction algorithms (Li et al., 2020). Amanita implants incorporate these advances with a bio-inspired, parametric design that supports on-site manufacturing and seamless integration with automated systems. The lattice structure (Fig. 3) plays a dual role: housing BAG and enhancing deformation under load, which aids impact absorption and ensures better compliance with cranial bones (Kulkova, 2023). A bio-inspired cranial implant structure, conceptually similar to ours, was reported by (Sharma et al., 2021b). However, they faced significant challenges in extrusive printing of a spatial 3D structure, ultimately suggesting powder-based methods as more suitable (Sharma et al., 2021b). In contrast, our approach reverse engineers the 3D implant shape into a 2D form for flat printing, a method first proposed by the same group (Sharma et al., 2021c). This eliminates some of the reported challenges, facilitates the incorporation of BAG granules during printing, and allows reformation into the original 3D shape via adaptive moulding. This method is particularly effective for Amanita "on-lay" implants, which have higher tolerance margins than "in-lay" types. Examples of 3D-printed Amanita implants are shown in Fig. 8.

5. Conclusion

This study introduced the design of a novel cranial implant integrating bionic principles and AM with PEEK and S53P4 bioactive glass. The Amanita implants demonstrated promising mechanical performance, exceeding baseline requirements for patient safety and effectiveness in cranial reconstructive surgery, though further studies and clinical trials are needed to confirm their full potential.

Disclosures

Authors NM, JK, JF and KA are minority shareholders in Ambrocio Oy. Author JK is employed by Ambrocio Oy.

CRediT authorship contribution statement

Dylan Coyle: Writing – Original Draft, Methodology, Software, Investigation, Formal analysis.

Bianca Zumbo: Methodology, Investigation, Writing – Review & Editing, Visualization.

Niko Moritz: Conceptualization, Project administration, Funding acquisition, Supervision, Writing – Original Draft, Methodology, Formal analysis, Validation.

Janek Frantzén: Conceptualization, Writing – Review & Editing.

Kalle Aitasalo: Conceptualization.

Gianluca Turco: Conceptualization, Supervision, Validation, Writing – Review & Editing.

Julia Kulkova: Conceptualization, Funding acquisition, Supervision, Resources, Methodology, Validation, Writing – Review & Editing.

IRB/ethics committee approval statement

This study did not require approval from an Institutional Review

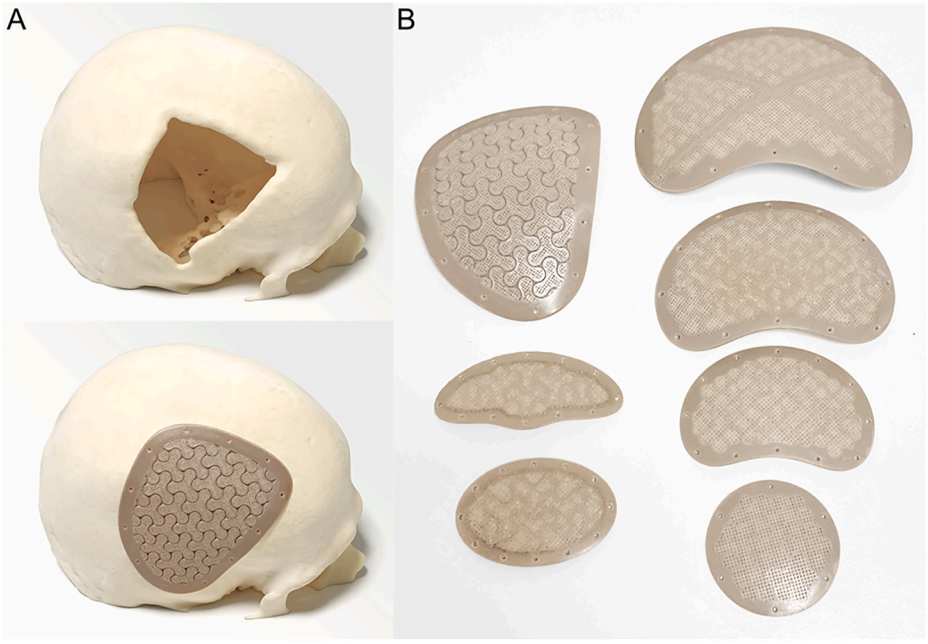

Fig. 8. A) Patient specific version of 3D-printed Amanita implant; B) Various versions of 3D-printed temporal and frontal Amanita implant.

Board (IRB) or Ethics Committee, as it is purely experimental and does not involve testing on animals or human participants. The research focuses on identifying the optimal mechanical design for the production of resistant cranial implants.

Declaration of generative AI and AI-assisted technologies in the writing process

Statement: During the preparation of this work the author(s) used [ChatGPT 4] to improve the readability and language of the manuscript. After using this tool, the author(s) reviewed and edited the content as needed and take(s) full responsibility for the content of the published article.

Funding

Author NM acknowledges the grant from The Jane and Aatos Erkko Foundation, "Additive manufacturing of osteoconductive composite implants".

References

Aitasalo, K.M.J., Piitulainen, J.M., Rekola, J., Vallittu, P.K., 2014. Craniofacial bone reconstruction with bioactive fiber-reinforced composite implant: bioactive fiber-reinforced composite implant. Head Neck 36 (5), 722–728. https://doi.org/10.1002/hed.23370.

Aydin, S., Kucukyuruk, B., Abuzayed, B., Aydin, S., Sanus, G.Z., 2011. Cranioplasty: review of materials and techniques. J. Neurosci. Rural Pract. 2 (2), 162–167. https://doi.org/10.4103/0976-3147.83584.

Berretta, S., Evans, K., Ghita, O., 2018. Additive manufacture of PEEK cranial implants: manufacturing considerations versus accuracy and mechanical performance. Mater. Des. 139, 141–152. https://doi.org/10.1016/j.matdes.2017.10.078.

Cong, B., Zhang, H., 2025. Innovative 3D printing technologies and advanced materials revolutionizing orthopedic surgery: current applications and future directions. Front. Bioeng. Biotechnol. 13, 1542179. https://doi.org/10.3389/fbioe.2025.1542179.

De Bonis, P., Frassanito, P., Mangiola, A., Nucci, C.G., Anile, C., Pompucci, A., 2012. Cranial repair: how complicated is filling a "hole". J. Neurotrauma 29 (6), 1071–1076. https://doi.org/10.1089/neu.2011.2116.

Di Cosmo, L., Pellicanò, F., Choueiri, J.E., Schifino, E., Stefini, R., Cannizzaro, D., 2025. Meta-analyses of the surgical outcomes using personalized 3D-printed titanium and PEEK vs. Standard implants in cranial reconstruction in patients undergoing craniectomy. Neurosurg. Rev. 48 (1), 312. https://doi.org/10.1007/s10143-025-03470-9.

Ebel, F., Schön, S., Sharma, N., Guzman, R., Mariani, L., Thieringer, F.M., Soleman, J., 2023. Clinical and patient-reported outcome after patient-specific 3D printer-assisted cranioplasty. Neurosurg. Rev. 46 (1), 93. https://doi.org/10.1007/s10143-023-02000-9.

Elshazly, N., Nasr, F.E., Hamdy, A., Saied, S., Elshazly, M., 2024. Advances in clinical applications of bioceramics in the new regenerative medicine era. World J. Clin. Cases 12 (11), 1863–1869. https://doi.org/10.12998/wjcc.v12.i11.1863.

Evonic CaP-loaded Vestakeep. https://products.evonik.com/assets/34/93/VESTAKEEP_Polymers_for_Medical_Applications_EN_EN_243493.pdf.

Evonic Vestakeep i4. https://products.evonik.com/assets/34/93/VESTAKEEP_Polymers_for_Medical_Applications_EN_EN_243493.pdf.

Huys, S.E.F., Van Gysel, A., Mommaerts, M.Y., Sloten, J.V., 2021. Evaluation of patient-specific cranial implant design using finite element analysis. World Neurosurg. 148, 198–204. https://doi.org/10.1016/j.wneu.2021.01.102.

Jaberi, J., Gambrell, K., Tiwana, P., Madden, C., Finn, R., 2013. Long-term clinical outcome analysis of poly-methyl-methacrylate cranioplasty for large skull defects. J. Oral Maxillofac. Surg. 71 (2), e81–e88. https://doi.org/10.1016/j.joms.2012.09.023.

Kauke-Navarro, M., Knoedler, L., Knoedler, S., Deniz, C., Stucki, L., Safi, A.-F., 2024. Balancing beauty and science: a review of facial implant materials in craniofacial surgery. Front. Surg. 11, 1348140. https://doi.org/10.3389/fsurg.2024.1348140.

Khalid, S.I., Thomson, K.B., Maasarani, S., Wiegmann, A.L., Smith, J., Adogwa, O., Mehta, A.I., Dorafshar, A.H., 2022. Materials used in cranial reconstruction: a systematic review and meta-analysis. World Neurosurg. 164, e945–e963. https://doi.org/10.1016/j.wneu.2022.05.073.

Kulkova, Y., 2023. Affordable Bionic Semi-patient-specific Cranial Implants for Low- and Middle-Income Countries and Conflict Zones.

Li, J., Pepe, A., Gsaxner, C., Campe, G. von, Egger, J., 2020. A baseline approach for autoimplant: the MICCAI 2020 cranial implant design challenge (arXiv: 2006.12449). arXiv. http://arxiv.org/abs/2006.12449.

Liaw, C.-Y., Tolbert, J.W., Chow, L.W., Guvendiren, M., 2021. Interlayer bonding strength of 3D printed PEEK specimens. Soft Matter 17 (18), 4775–4789. https://doi.org/10.1039/D1SM00417D.

Lindfors, N.C., Hyvönen, P., Nyyssönen, M., Kirjavainen, M., Kankare, J., Gullichsen, E., Salo, J., 2010a. Bioactive glass S53P4 as bone graft substitute in treatment of osteomyelitis. Bone 47 (2), 212–218. https://doi.org/10.1016/j.bone.2010.05.030.

Lindfors, N.C., Koski, I., Heikkilä, J.T., Mattila, K., Aho, A.J., 2010b. A prospective randomized 14-year follow-up study of bioactive glass and autogenous bone as bone graft substitutes in benign bone tumors. J. Biomed. Mater. Res. B Appl. Biomater. 94B (1), 157–164. https://doi.org/10.1002/jbm.b.31636.

Magni, F., Al-Omari, A., Vardanyan, R., Rad, A.A., Honeyman, S., Boukas, A., 2024. An update on a persisting challenge: a systematic review and meta-analysis of the risk factors for surgical site infection post craniotomy. Am. J. Infect. Control 52 (6), 650–658. https://doi.org/10.1016/j.ajic.2023.11.005.

Mah, J., Kass, R., 2016. The impact of cranioplasty on cerebral blood flow and its correlation with clinical outcome in patients underwent decompressive craniectomy. Asian J. Neurosurg. 11 (1), 15–21. https://doi.org/10.4103/1793-5482.172593.

Marcián, P., Narra, N., Borák, L., Chamrad, J., Wolff, J., 2019. Biomechanical performance of cranial implants with different thicknesses and material properties: a finite element study. Comput. Biol. Med. 109, 43–52. https://doi.org/10.1016/j.compbiomed.2019.04.016.

Miguez-Pacheco, V., Hench, L.L., Boccaccini, A.R., 2015. Bioactive glasses beyond bone and teeth: emerging applications in contact with soft tissues. Acta Biomater. 13, 1–15. https://doi.org/10.1016/j.actbio.2014.11.004.

Moiduddin, K., Mian, S.H., Elseufy, S.M., Alkhalefah, H., Ramalingam, S., Sayeed, A., 2023. Polyether-ether-ketone (PEEK) and its 3D-printed quantitate assessment in cranial reconstruction. J. Funct. Biomater. 14 (8), 429. https://doi.org/10.3390/jfb14080429.

Munukka, E., Leppäranta, O., Korkeamäki, M., Vaahtio, M., Peltola, T., Zhang, D., Hupa, L., Ylänen, H., Salonen, J.I., Viljanen, M.K., Eerola, E., 2008. Bactericidal effects of bioactive glasses on clinically important aerobic bacteria. J. Mater. Sci. Mater. Med. 19 (1), 27–32. https://doi.org/10.1007/s10856-007-3143-1.

Ono, I., Tateshita, T., Nakajima, T., Ogawa, T., 1998. Determinations of strength of synthetic hydroxyapatite ceramic implants. Plast. Reconstr. Surg. 102 (3), 807–813. https://doi.org/10.1097/00006534-199809010-00027.

OssDsign, A.B., 2021. OSSDSIGN Cranial PSI, (510(k)). https://www.accessdata.fda.gov/scripts/cdrh/cfdocs/cfpmn/pmn.cfm?ID=K212414.

Persson, J., Helgason, B., Engqvist, H., Ferguson, S.J., Persson, C., 2018. Stiffness and strength of cranioplastic implant systems in comparison to cranial bone. J. Cranio-Maxillofacial Surg. 46 (3), 418–423. https://doi.org/10.1016/j.jcms.2017.11.025.

Piitulainen, J.M., Mattila, R., Moritz, N., Vallittu, P.K., 2017. Load-bearing capacity and fracture behavior of glass fiber-reinforced composite cranioplasty implants. J. Appl. Biomater. Funct. Mater. 15 (4), e356–e361. https://doi.org/10.5301/jabfm.5000375.

Pöppe, Johannes P., Spendel, M., Griessenauer, C.J., Gaggl, A., Wurm, W., Enzinger, Simon, 2024. Point-of-Care 3-dimensional–printed polyetheretherketone customized implants for cranioplastic surgery of large skull defects. Oper. Neurosurg. 27 (4), 449–454. https://doi.org/10.1227/ons.0000000000001154.

Punchak, M., Chung, L.K., Lagman, C., Bui, T.T., Lazareff, J., Rezzadeh, K., Jarrahy, R., Yang, I., 2017. Outcomes following polyetheretherketone (PEEK) cranioplasty: systematic review and meta-analysis. J. Clin. Neurosci. 41, 30–35. https://doi.org/10.1016/j.jocn.2017.03.028.

Sharma, N., Aghlmandi, S., Dalcanale, F., Seiler, D., Zeilhofer, H.-F., Honigmann, P., Thieringer, F.M., 2021a. Quantitative assessment of point-of-care 3D-printed patient-specific polyetheretherketone (PEEK) cranial implants. Int. J. Mol. Sci. 22 (16), 8521. https://doi.org/10.3390/ijms22168521.

Sharma, N., Ostas, D., Rotar, H., Brantner, P., Thieringer, F.M., 2021b. Design and additive manufacturing of a biomimetic customized cranial implant based on voronoi diagram. Front. Physiol. 12, 647923. https://doi.org/10.3389/fphys.2021.647923.

Sharma, N., Welker, D., Aghlmandi, S., Maintz, M., Zeilhofer, H.-F., Honigmann, P., Seifert, T., Thieringer, F.M., 2021c. A multi-criteria assessment strategy for 3D printed porous polyetheretherketone (PEEK) patient-specific implants for orbital wall reconstruction. J. Clin. Med. 10 (16), 3563. https://doi.org/10.3390/jcm10163563.

Sun, C., Kang, J., Yang, C., Zheng, J., Su, Y., 2022. Additive Manufactured Polyether-Ether-Ketone Implants for Orthopaedic Applications: A Narrative Review.

Sundblom, J., Gallinetti, S., Birgersson, U., Engqvist, H., Kihlström, L., 2019. Gentamicin loading of calcium phosphate implants: implications for cranioplasty. Acta Neurochir. 161 (6), 1255–1259. https://doi.org/10.1007/s00701-019-03895-4.

Välimäki, V.-V., Aro, H.T., 2006. Molecular basis for action of bioactive glasses as bone graft substitute. Scand. J. Surg. 95 (2), 95–102. https://doi.org/10.1177/145749690609500204.

Vallittu, P.K., Posti, J.P., Piitulainen, J.M., Serlo, W., Määttä, J.A., Heino, T.J., Pagliari, S., Syrjänen, S.M., Forte, G., 2020. Biomaterial and implant induced ossification: in vitro and in vivo findings. J. Tissue Eng. Regen. Med. 14 (8), 1157–1168. https://doi.org/10.1002/term.3056.

Van De Vijfeijken, S.E.C.M., Münker, T.J.A.G., Spijker, R., Karssemakers, L.H.E., Vandertop, W.P., Becking, A.G., Ubbink, D.T., Becking, A.G., Dubois, L., Karssemakers, L.H.E., Milstein, D.M.J., Van De Vijfeijken, S.E.C.M., Depauw, P.R.A.M., Hoefnagels, F.W.A., Vandertop, W.P., Kleverlaan, C.J., Münker, T.J.A.G., Maal, T.J.J., Nout, E., et al., 2018. Autologous bone is inferior to alloplastic cranioplasties: safety of autograft and allograft materials for cranioplasties, a systematic review. World Neurosurg. 117, 443–452.e8. https://doi.org/10.1016/j.wneu.2018.05.193.

Van Lierde, C., Depreitere, B., Vander Sloten, J., Van Auderkercke, R., Van Der Perre, G., Goffin, J., 2003. Skull biomechanics: The energy absorbability of the human skull frontal bone during fracture under quasi-static loading. J. Appl. Biomater. Biomech. 1 (3), 194–199. PMID: 20803457.

Wang, Y., Müller, W.-D., Rumjahn, A., Schmidt, F., Schwitalla, A.D., 2021. Mechanical properties of fused filament fabricated PEEK for biomedical applications depending on additive manufacturing parameters. J. Mech. Behav. Biomed. Mater. 115, 104250. https://doi.org/10.1016/j.jmbbm.2020.104250.

Zadpoor, A.A., 2020. Meta-biomaterials. Biomater. Sci. 8 (1), 18–38. https://doi.org/10.1039/C9BM01247H.

Zhang, Q., Yuan, Y., Li, X., Sun, T., Zhou, Y., Yu, H., Guan, J., 2018. A large multicenter retrospective research on embedded cranioplasty and covered cranioplasty. World Neurosurg. 112, e645–e651. https://doi.org/10.1016/j.wneu.2018.01.114.

Zhao, D., Moritz, N., Vedel, E., Hupa, L., Aro, H.T., 2008. Mechanical verification of soft-tissue attachment on bioactive glasses and titanium implants. Acta Biomater. 4 (4), 1118–1122. https://doi.org/10.1016/j.actbio.2008.02.012.